Neuron
Report

Analysis of Excitatory Microcircuitry in the Medial Entorhinal Cortex Reveals Cell-Type-Specific Differences

Prateep Beed,[1,7] Michael H.K. Bendels,[2,7] Hauke F. Wiegand,[1] Christian Leibold,[4,5] Friedrich W. Johenning,[1,8,*] and Dietmar Schmitz[1,3,6,8,*]
[1]Neuroscience Research Center
[2]Neurophysics Group, Department of Neurology
[3]Cluster of Excellence "NeuroCure"
Charité-Universitätsmedizin Berlin, 10117 Berlin, Germany
[4]Bernstein Center for Computational Neuroscience Munich, Großhaderner Str. 2, 82152 Planegg-Martinsried, Germany
[5]Division of Neurobiology, Ludwig-Maximilians-Universität München, Großhaderner Str. 2, 82152 Planegg-Martinsried, Germany
[6]Bernstein Center for Computational Neuroscience Berlin, Philippstr. 13, 10115 Berlin, Germany
[7]These authors contributed equally to this work
[8]These authors contributed equally to this work
*Correspondence: friedrich.johenning@charite.de (F.W.J.), dietmar.schmitz@charite.de (D.S.)
DOI 10.1016/j.neuron.2010.12.009

SUMMARY

Medial entorhinal cortex (MEC) plays an important role in physiological processes underlying navigation, learning, and memory. Excitatory cells in the different MEC layers project in a region-specific manner to the hippocampus. However, the intrinsic microcircuitry of the main excitatory cells in the superficial MEC layers is largely unknown. Using scanning photostimulation, we investigated the functional microcircuitry of two such cell types, stellate and pyramidal cells. We found cell-type-specific intralaminar and ascending interlaminar feedback inputs. The ascending interlaminar inputs display distinct organizational principles depending on the cell-type and its position within the superficial lamina: the spatial spread of inputs for stellate cells is narrower than for pyramidal cells, while inputs to pyramidal cells in layer 3, but not in layer 2, exhibit an asymmetric offset to the medial side of the cell's main axis. Differential laminar sources of excitatory inputs might contribute to the functional diversity of stellate and pyramidal cells.

INTRODUCTION

The medial entorhinal cortex (MEC) is a six-layered cortex and is part of the medial temporal lobe. It is implicated in physiological processes underlying navigation, learning, and memory and is often the site for early insults during pathophysiological conditions such as epilepsy and Alzheimer disease (Canto et al., 2008; Witter and Amaral, 2004). The superficial layers of the MEC contain two morphologically distinct excitatory projection neurons: the stellate and the pyramidal cells. Layer 2 (L2) contains both stellate and pyramidal cells (L2Ss and L2Ps respectively; Alonso and Klink, 1993), whereas layer 3 (L3) is exclusively composed of pyramidal cells (L3Ps) as projection neurons (Dickson et al., 1997; Gloveli et al., 1997).

MEC is the main input relay to the hippocampus. The main excitatory cells in the superficial layers project in a region-specific manner to the hippocampus. Although such interregional connectivity has long been studied, not much is known about the intrinsic organization of the microcircuitry in the MEC. Microcircuits are characterized by the cell-specific ratios of intralaminar and interlaminar connections and the spatial distribution of inputs (Lübke and Feldmeyer, 2007; Mountcastle, 1997; Schubert et al., 2007). Anatomical and electrophysiological studies have distinguished two different patterns of associative connectivity in superficial layers of the MEC: intralaminar recurrent connections (Köhler, 1986; Dhillon and Jones, 2000) and ascending interlaminar feedback connections (Iijima et al., 1996; Kloosterman et al., 2003; Köhler, 1986). Those studies, however, have not revealed the target-cell-specific functional connectivity patterns with respect to the layer-specific weight and spatial organization of the microcircuitry for all three classes of superficial excitatory cells.

Using scanning photostimulation with caged glutamate (Callaway and Katz, 1993), we mapped the microcircuitry of the excitatory cells in the L2-3 MEC. Our mapping experiments show that in the entorhinal cortex, different cell types within the same layer display a cell-type-specific distribution of intralaminar recurrent connections (superficial to superficial microcircuit) and ascending interlaminar feedback connections (deep to superficial microcircuit). We show that the connections from deep to superficial excitatory cells are organized in spatial input clusters and analyze the spatial distribution of these input clusters. Their horizontal diameter of such spatial input clusters is determined by the cell type of the target cell. We further observe a striking asymmetry of the deep to superficial microcircuitry: cells located deeper on a vertical axis display a more asymmetric medial offset of their deep input clusters.

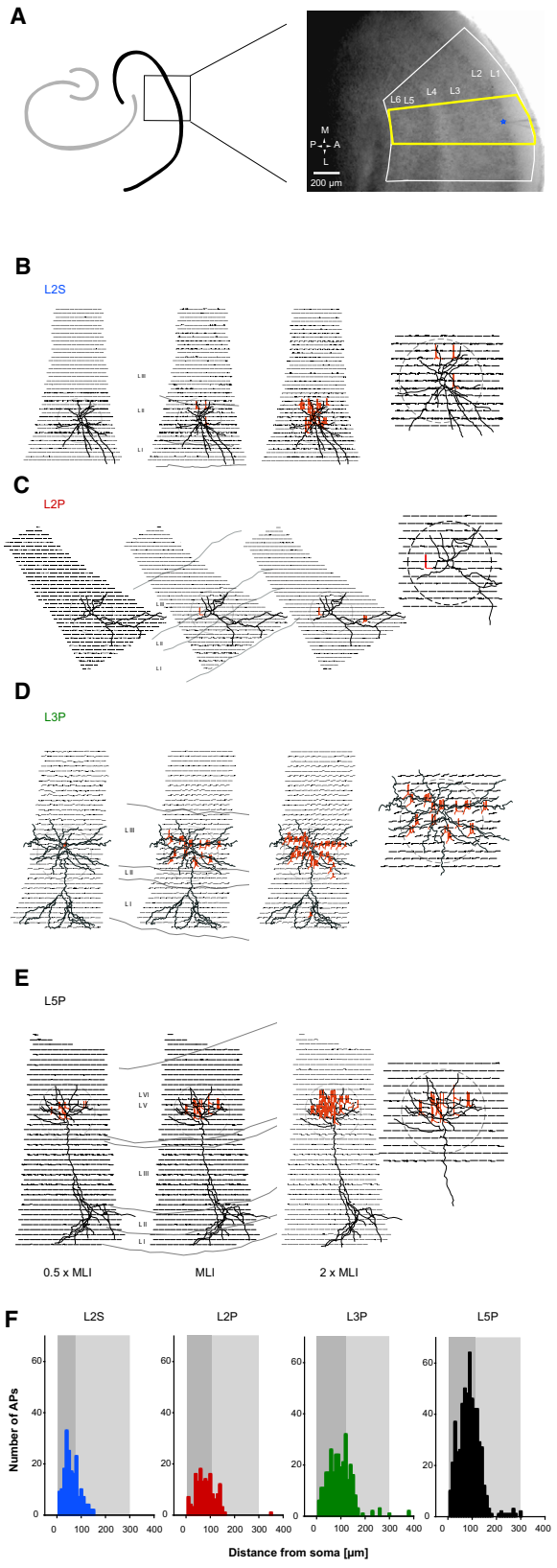

Figure 1. Resolution of Photoactivation by Glutamate Uncaging

(A) Horizontal acute brain slices containing the hippocampal formation were used for the mapping experiments. The MEC is highlighted in the DIC image. The yellow polygon indicates the area for mapping AP profiles and the white polygon indicates the area for mapping synaptic connections. (B–E) Spatial profiles of excitability of the main excitatory cells were performed. The stimulation pattern consisted of points with 30 μm spacing, and the area mapped is indicated by the yellow polygon in (A). The voltage changes elicited at each stimulus site were plotted and overlayed with Neurolucida reconstructions and shown for three laser intensities (0.5× mapping laser intensity [MLI], MLI, and 2× MLI). Subthreshold responses are depicted in black and suprathreshold responses in red. (B) L2S, (C) L2P, (D) L3P, (E) layer 5/6 pyramidal cell (L5P). On the rightmost panel, the perisomatic region is zoomed in for the MLI trial. (F) Analysis of excitation profiles; excitability in response to photostimulation as indicated by the number of APs per 10 μm spatial bin, shown for each cell type. The dark gray shading corresponds to d*, where 75% of all inputs were observed. The lighter gray shading depicts a distance of 300 μm from the cell soma.

Cells in the different superficial layers of the MEC project to specific output stations in the hippocampus and are also differentially involved and/or modulated in various pathophysiological insults. Therefore, knowledge of the cell-type-specific microcircuitry is crucial for understanding function and dysfunction of the hippocampal formation.

RESULTS

Calibration of Spatial Profiles of Excitatory Cells in the Medial Entorhinal Cortex

Focal photolysis of caged glutamate induces two types of activity in the recorded neuron, direct and indirect synaptic responses. The direct responses were evoked when glutamate was uncaged directly on the cell soma or the dendrites of the recorded cell. Indirect synaptic responses reflect suprathreshold activation that results in action potential (AP) firing of a presynaptic cell projecting onto the recorded cell (Figures 1 and 2).

The first step was to determine the laser intensity that permits maximal spatial resolution when mapping indirect synaptic inputs. A measure of spatial resolution for scanning photostimulation is the critical distance d*, which is defined as the distance from the cell soma where 75% of all cumulated action potentials were evoked as direct responses. The d* value depends on cell type and laser intensity. It enables extrapolation of the distance between cell soma and dendritic hotspots, i.e., the location on the dendritic arbours from which an AP is evoked by photolysis of caged glutamate (Bendels et al., 2008; Shepherd et al., 2003). In Figure 1A, the MEC is displayed in the differential interference contrast (DIC) image. The yellow rectangle represents the area scanned for calibration of spatial firing profile. Such spatial profiles of AP firing of the main excitatory cells in all layers of the MEC were generated in the current-clamp mode. In Figures 1B–1E, camera lucida reconstructions of representative cells were overlayed with subthreshold (black) and suprathreshold (red) direct responses elicited at each stimulus site. The stimulation pattern consisted of points with 30 μm spacing. For each cell type, d* was calculated at different laser intensities. We observed perisomatic clustering of suprathreshold inputs (Figures 1B–1E). Analysis of the spatial distribution of direct

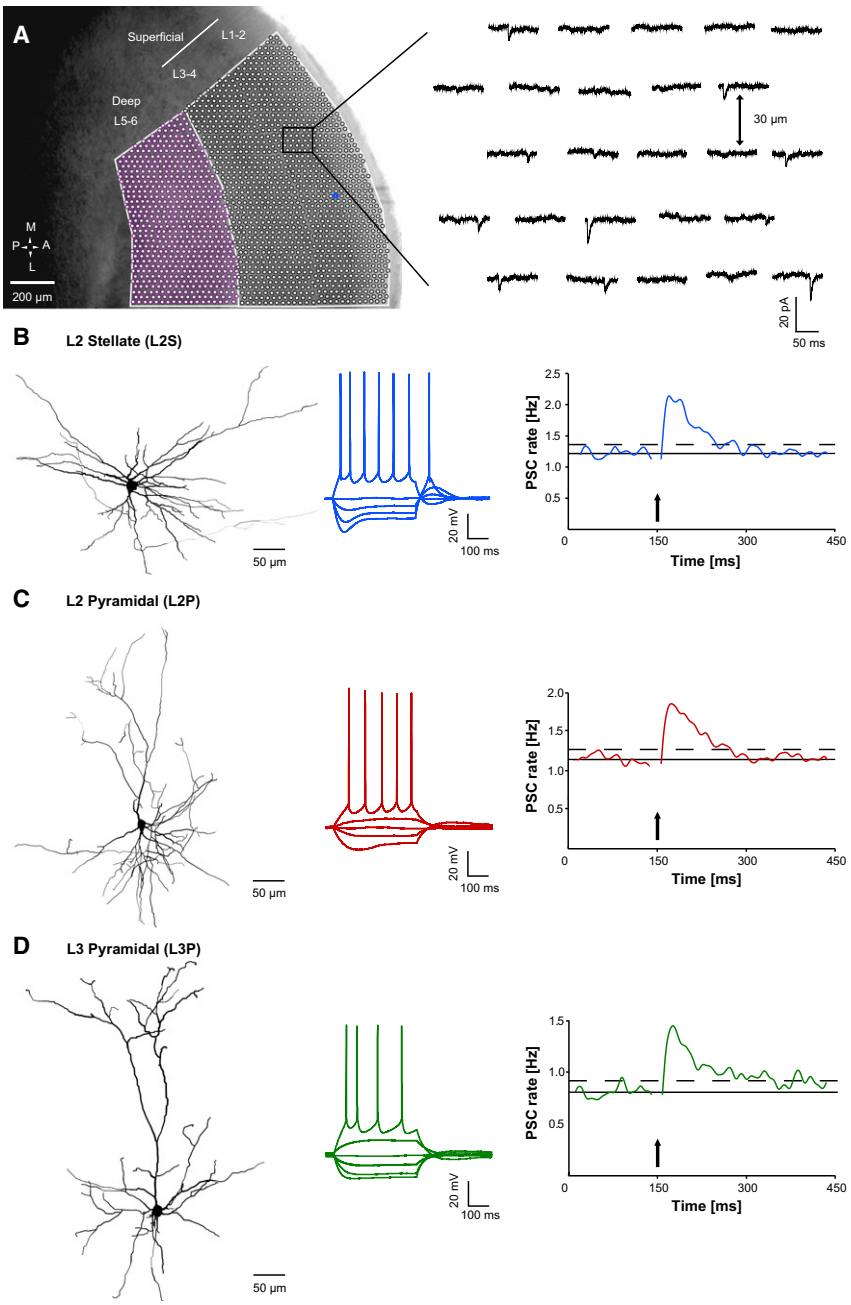

Figure 2. Mapping Excitatory Cells in the Superficial MEC

(A) Scanning raster (left) superimposed on the DIC image of the entorhinal cortex. The cortical region was grouped into the following layers: L1–L4 (black, superficial inputs) and L5–L6 (purple, deep inputs). The raster consisted of stimulation points separated by 30 μm, and the trials were randomized to avoid any bias arising from scanning these cortical layers in a fixed order. Traces from the 5 × 5 raster highlighted in (A) are displayed on the right. The first 100 ms after the UV-flash are plotted at each stimulation point. (B–D) Biocytin reconstructions (left) of representative (B) L2S, (C) L2P, and (D) L3P. Corresponding electrophysiological properties (middle) of these two main projection neurons in the L2 MEC are shown. Average postsynaptic current (PSC) incidence rates are indicated (right). Arrows indicate the time-points of the UV flash.

APs in maps with a large scanning field (Figure 1A) shows that almost all suprathreshold inputs could be detected within 300 μm distance from the soma (L2S: 100% [n = 5]; L2P: 99.3 ± 0.7% [n = 6]; L3P: 96 ± 4% [n = 5]; L5P: 100% [n = 5]). In Figure 1F, we have plotted the number of APs in dependence on the distance from the cell soma. Recordings were done for each cell type at the laser intensity used for our experiments. To calculate d*, we pooled these large scanning region calibration maps with maps using a 150 μm perisomatic radius. The resulting cell-type-specific d* values were as follows: L2 stellate cell (n = 23), 74.2 μm; L2 pyramidal cell (n = 18), 102.1 μm; L3 pyramidal cell (n = 24), 119.2 μm; and L5/6 pyramidal cell (L5P, n = 31), 109.9 μm (Figure 1F).

Mapping Excitatory Cells in the Superficial MEC

To determine the functional microcircuitry, mapping of synaptic inputs was performed for the main excitatory cells in the superficial MEC, the L2S, the L2P, and the L3P cells (Alonso and Klink, 1993). For the mapping experiments, a hexagonal grid was projected across the different layers in the entorhinal cortex. Figure 2A depicts the mapping area. The scanning region (L1–L6) was grouped into the following cortical layers: superficial layers (L1–L4, black) and deep layers (L5–L6, purple; Figure 2A).

The two cell types in L2 were identified by their characteristic morphological and electrophysiological properties. The mapped cells could be categorized based on their biophysical properties (larger hyperpolarizing and depolarizing sag current and early firing upon depolarization for L2Ss, small hyperpolarizing and depolarizing sag current and slow ramp current with long-latency AP firing upon depolarization for L2Ps; Figures 2B and 2C left and middle; Alonso and Klink, 1993). The L3P were easily identified based on their laminar location and uniform distribution in layer 3 (Figure 2D).

Uncaging of glutamate evoked both direct and indirect synaptic responses. These were clearly separated by their different delay-to-onset times. Direct responses were elicited almost immediately (in a time window of 10 ms), whereas synaptic inputs were collected up to 95 ms following ultraviolet (UV) photolysis (see Figures 2B and 2C, right; see Bendels et al., 2008 for details). In order to discriminate between photo-induced synaptic input

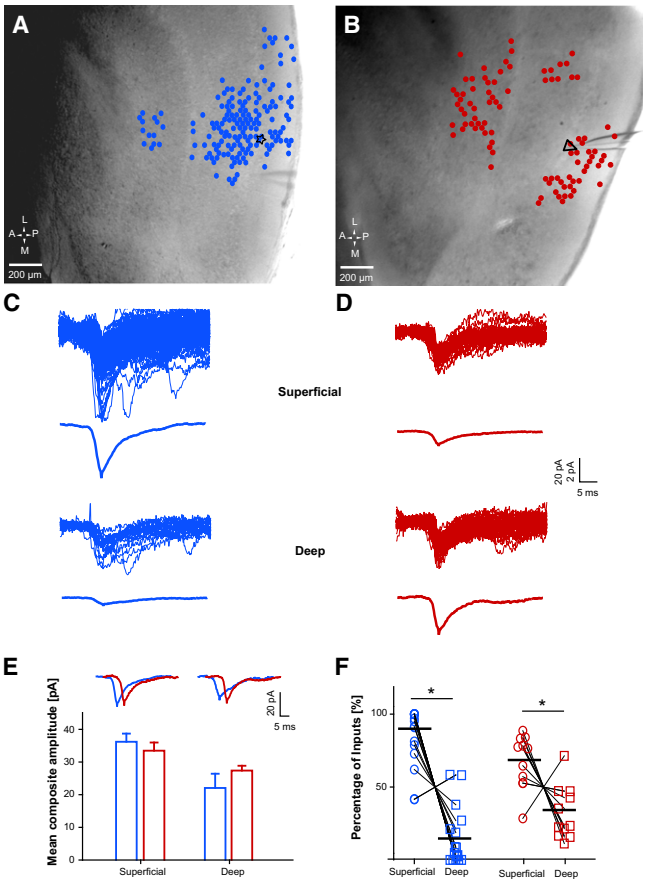

Figure 3. Cell-Type-Specific Microcircuitry for L2 MEC Excitatory Cells

(A) Blue dots highlight the uncaging spots that were detected as synaptic points projecting to the L2S (black star) from a single representative map. Most of the inputs of this L2S arise from intralaminar recurrent connections. (B) Red dots highlight all uncaging spots that were detected as synaptic points projecting to the L2P (black triangle) from a single representative map. The L2P receives less superficial intralaminar recurrent connections but receives stronger ascending interlaminar feedback connections from the deep layers of the MEC. (C and D) Indirect synaptic responses underlying the synaptic points in (C) the L2S in (A) and (D) the L2P in (B) were aligned to the minimum. The overlays correspond to superficial (top) and deep (bottom) lamina. The corresponding average traces are scaled to the total number of scanned points (including all uncaging points which were not synaptic points) in each lamina to document differences in input strength. (E) Mean composite synaptic amplitude as the sum of synaptic current amplitudes divided by the number of points from which a synaptic response was detected, calculated for each cell in the different layers. L2S: blue columns; L2P: red columns. Within layers, the differences are not statistically significant ($p > 0.05$, Mann-Whitney U test). (Inset) Traces are unscaled averages of the synaptic inputs depicted in the overlays in (C) and (D). (F) Quantification of input source location for both L2S and L2P. The percentage of synaptic points in the different layers as a fraction of the total number of synaptic points is calculated for each cell. Circles indicate the percentage of inputs coming from the superficial layers for each cell analyzed; squares indicate the same for deep inputs. L2S, blue (n = 15); L2P, red (n=11; L2S versus L2P: $p>0.05$, Mann-Whitney U test; values are reported as mean ± SEM). For both cell types, the percentage of superficial layer input was significantly higher than deep layer inputs ($p < 0.05$, Mann-Whitney U test). When comparing across cell types, L2Ss receive a significantly higher proportion of inputs from the superficial lamina ($p < 0.05$, Mann-Whitney U test), whereas L2Ps receive a significantly higher proportion of inputs from the deep lamina ($p < 0.05$, Mann-Whitney U test).

points and background activity, we used a spatial-correlation-based algorithm to extract presynaptic input locations that were termed synaptic points. (Bendels et al., 2010; for details see Experimental Procedures). Further, to exclude the effect of dendritic filtering biasing the detection of somatic EPSCs by the automatic detection algorithm, we applied localized puffs of sucrose at distinct distal dendritic locations in L2Ps and L2Ss. The algorithm was able to faithfully detect EPSCs from distal dendritic locations (for details see Supplemental Experimental Procedures and Figure S1, available online).

Distribution of Inter- and Intralaminar Synaptic Inputs onto L2Ss and L2Ps

We started our analysis of the microcircuitry of the two main excitatory cells in the L2 MEC by analyzing the ratio of superficial to superficial and deep to superficial connectivity. This ratio is derived from input maps in which synaptic points were plotted for the different cell types (Figures 3A and 3B). We calculated the mean composite synaptic amplitude (sum of photoactivation-induced synaptic current amplitudes divided by number of points from which a synaptic response was detected), from each layer for each cell and then compared these values between cell types. We could not detect significant differences between L2Ps and L2Ss for the strength of input from either the deep or superficial layers (Figure 3E; superficial: 36.18 ± 2.5 pA for L2Ss [n = 15] versus 33.46 ± 2.5 pA for L2Ps [n = 11], $p > 0.05$, Mann-Whitney U test; deep: 22.06 ± 4.35 pA for L2Ss [n = 15] versus 27.38 ± 1.47 pA for L2Ps [n = 11], $p > 0.05$, Mann-Whitney U test). We therefore decided to base our microcircuit analysis on a digital readout of synaptic inputs (Figures 3A and 3B), thereby reducing the variability introduced by the analog readout via probabilistic synaptic transmission.

As shown in Figures 3A to 3D, there are differences in the relative amount of deep to superficial and superficial to superficial connections for L2Ss and the L2Ps. For each cell, we also calculated the percentage of synaptic points in the different layers as a fraction of the total number of synaptic points. Among the L2S population, on average, 83.55 ± 5.30% of all synaptic points arise from the superficial layers while only 16.45 ± 5.30% arise from the deep layers (n = 15). For L2Ps, 67.7 ± 5.51% of synaptic points are from the superficial layers and 32.3 ± 5.51% from deep layers (n = 11; Figure 3F). Comparing deep and superficial inputs within cell types, both L2Ss and L2Ps receive significantly more input from the superficial layers than from the deep layers (Figure 3F; L2P superficial versus deep: $p < 0.05$; L3P superficial versus deep: $p < 0.05$; Mann-Whitney U test). Comparing superficial inputs between cell types, L2Ss receive significantly more superficial input than L2Ps (Figure 3F; $p < 0.05$, Mann-Whitney U test). In contrast, L2Ps receive significantly more deep layer input than L2Ss (Figure 3F; $p < 0.05$, Mann-Whitney U test). In fact, 7 out of 15 (46.67%) L2Ss received less than 5% of their total synaptic input from the deep layers, whereas every (11 out of 11) L2P received more than 10% of their inputs from the deep layers.

Spatial Organization of Ascending Interlaminar Feedback Connections

Microcircuit properties can be cell-type-specific or layer-specific (Schubert et al., 2007). In the MEC, we can differentiate

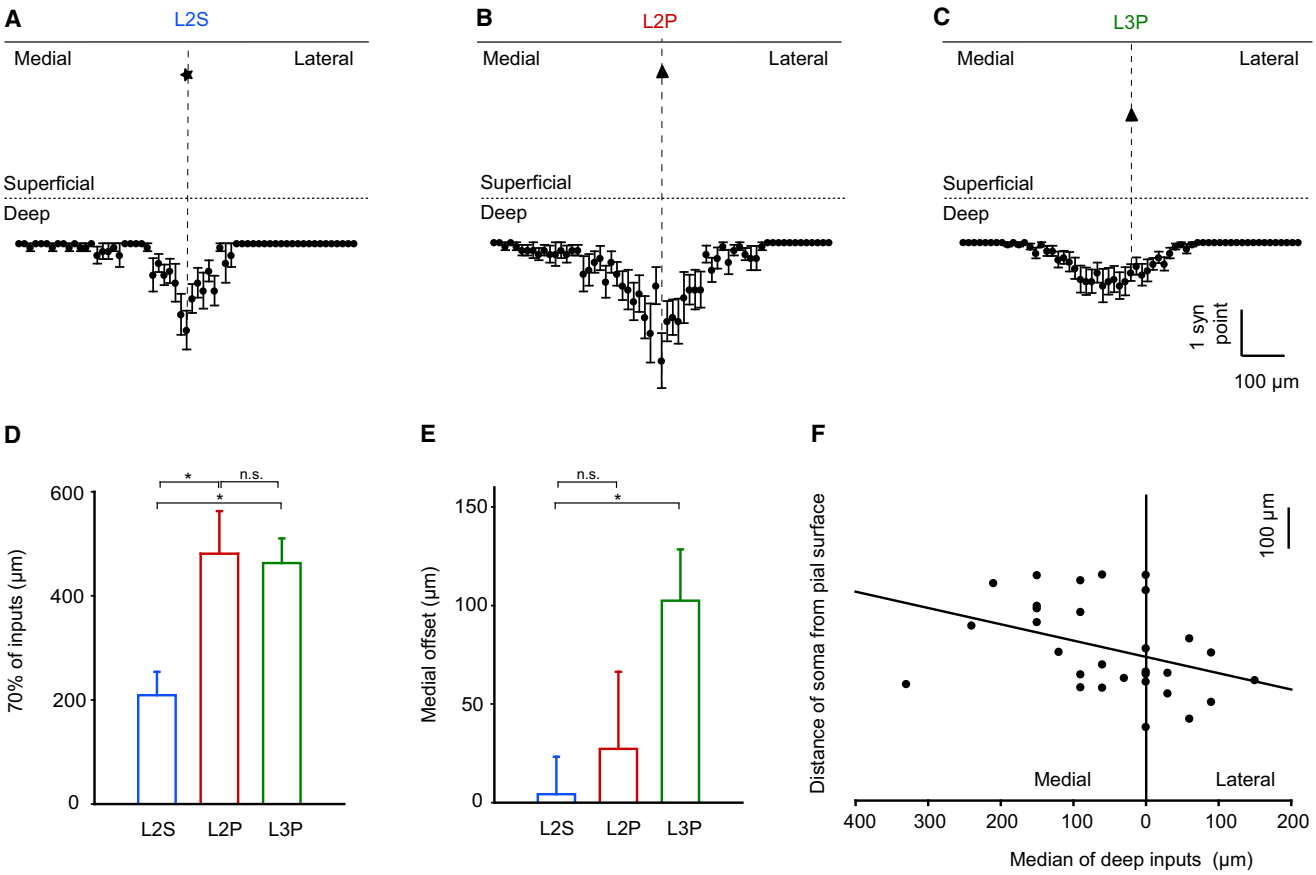

Figure 4. Modular Organization of Inputs in the MEC

(A–C) Average number of synaptic input points exclusively from the deep layers at different distances from the cell's main axis (perisomatic line perpendicular to the pial surface) to L2Ss (black star) in (A), L2Ps (black triangle) in (B), and L3Ps (black triangle) in (C). Values are reported as mean ± SEM. (D) Histogram compares the average spatial width in which we find 70% of all input points for all L2Ss (n = 7), L2Ps (n = 11), and L3Ps (n = 12). L2Ss received 70% of their deep layer inputs from a significantly smaller spatial distance than L2Ps and L3Ps (L2S versus L2P: $p < 0.05$; L2S versus L3P: $p < 0.05$; L2P versus L3P: $p > 0.05$; Kruskal-Wallis test with Dunn's Multiple Comparison; values are reported as mean ± SEM). (E) Histogram compares the offset of the deep layer input clusters from the cell's main axis by comparing the average median of all L2Ss (n = 7), L2Ps (n = 11), and L3Ps (n = 12). L2Ss display input cluster positioning on the main axis, which is significantly different from the medial offset observed for L3Ps (L2S versus L3P: $p < 0.05$, Mann-Whitney U test; values are reported as mean ± SEM). The average median of the more superficial population of L2Ps is only slightly shifted to the medial side and not significantly different from stellate cells (n = 11; L2S versus L2P: $p > 0.05$, Mann-Whitney U test). (F) Scatter plot displays the relationship between the distance of an excitatory cell (L2S, L2P, and L3P) soma from the pial surface and the spatial offset of the input cluster from the main axis quantified as the median of the deep input distance. The vertical position of an excitatory cell body in relation to the pial surface determines the offset (Pearson's $r = 0.38$, $p < 0.05$ ANOVA) of the input cluster from the main axis.

between the microcircuit organization of different cell types in the same layer (pyramidal and stellate cells in layer 2) and the same cell type in different layers (pyramidal cells in layer 2 and 3). To analyze the spatial organization of the deep to superficial microcircuitry, we aligned the input maps to the main axis of the cell. The main axis was constructed as a perisomatic axis perpendicular to the pial surface (Figures 4A–4C). The averaged maps of deep layer inputs revealed narrow single-peaked distributions for all cell types (Figures 4A–4C). The peak of the excitatory deep layer inputs is spatially confined close to the absolute position of the postsynaptic cell soma (see also Figures 3A and 3B). We refer to this spatial organization of deep to superficial microcircuitry as input clusters. The spatial organization of these input clusters displays both cell-type and layer-specific properties.

Compared to L2Ps and L3Ps, deep inputs to L2Ss display only half of the spatial spread around their main axis (Figures 4A–4C). L2Ss received 70% of their deep layer inputs within a spatial distance of 209 ± 45 µm from the main axis (n = 7, Figure 4D). L2Ps and L3Ps received the same fraction of inputs from a significantly wider spatial distance of 480.9 ± 82 µm (n = 11) and 462.9 ± 47 µm (n = 12), respectively (L2S versus L2P: $p < 0.05$; L2S versus L3P: $p < 0.05$; L2P versus L3P: $p > 0.05$; Kruskal-Wallis test with Dunn's Multiple Comparison; Figure 4D).

For L2Ss, the average median of all input clusters is positioned 4.3 ± 19 µm medial to the perisomatic axis perpendicular to the pial surface (n = 7; Figure 4E). In contrast to this input cluster positioning on the main axis of L2Ss, the average median of L3Ps displays a significant medial offset of 102.5 ± 26 µm (n = 12; L2S versus L3P: $p < 0.05$, Mann-Whitney U test; Figure 4E).

To exclude the possibility that this medial offset of the deep inputs is due to asymmetric distribution of dendritic arbours, we quantified the spatial spread of superficial inputs onto L3Ps. The average median of the superficial input is 47.8 ± 34 μm lateral to the main axis (n = 16). This slight lateral offset is significantly different from the medial offset of the deep inputs (L3P superficial versus L3P deep: $p < 0.05$, Mann-Whitney U test; Figure S3). The average median of deep inputs to the more superficial population of L2Ps is only slightly shifted to the medial side (27.3 ± 39 μm) and not significantly different from stellate cells (n = 11; L2S versus L2P: $p > 0.05$, Mann-Whitney U test; Figure 4E). When plotting the medians of the distance of stellate and pyramidal cell input clusters from the main axis against the distance of the cell soma from the pial surface, the depth of the soma is correlated with the medial offset (Pearson's $r = 0.38$, $p < 0.05$, ANOVA; Figure 4F). The asymmetric distribution of the input clusters with a medial offset toward the cell's main axis therefore results from a depth-dependent organization of interlaminar ascending inputs.

DISCUSSION

Scanning photostimulation permits functional characterization of microcircuits based on the number of target-cell-specific functional contacts (Callaway and Katz, 1993; Dalva and Katz, 1994). For large-scale mapping, scanning photostimulation has been mostly applied to primary sensory areas like the barrel cortex (Schubert et al., 2003; Shepherd et al., 2003) or visual cortex (Dantzker and Callaway, 2000). However, it seems that other cortical structures like the hippocampus exhibit distinct elements of microcircuit design, such as a specific topographic organization preserved between CA3 and CA1 subfields (Brivanlou et al., 2004).

We applied scanning photostimulation to study the microcircuitry of excitatory cells (stellate and pyramidal cells) in superficial layers of the MEC. L2Ss and L2Ps are predominantly embedded in superficial to superficial microcircuitry, with a larger fraction of deep to superficial microcircuitry for L2Ps. This deep to superficial microcircuitry is arranged in input clusters with a target-cell-specific spatial spread. A new element of microcircuit design is the asymmetric, medial offset of deep input clusters to L3Ps (not displayed by the superficial inputs onto L3Ps), which is correlated with a pyramidal cell's distance from the pial surface.

Based on anatomical studies, microcircuitry in the superficial MEC can be divided into two different pathways, the intralaminar recurrent connections and ascending interlaminar feedback connections (Köhler, 1986). Extracellular recordings and current source density analysis in vivo have been used to demonstrate ascending interlaminar feedback connections have been demonstrated primarily for deep layers to the superficial L3 (Kloosterman et al., 2003). Intralaminar recurrent connections have been demonstrated with paired recordings in L3 and L5 (Dhillon and Jones, 2000). In the same study, connected pairs of L2 cells could not be found, and interlaminar connectivity between the deep and superficial layers was not assessed. Another study reported a very low connectivity between L2Ss when using paired recordings (J.J. Couey et al., 2009, SFN Annual Meeting, abstract). When scanning photostimulation was used, intralaminar recurrent connections could be demonstrated in L2 (Kumar et al., 2007). We show that the two morphologically and biophysically different excitatory cell types in L2 MEC, L2Ss and L2Ps, (Alonso and Klink, 1993), are differentially embedded in the associative microcircuitry. Both L2Ss and L2Ps are mainly incorporated in superficial to superficial microcircuits, indicating recurrent connectivity both within L2 and from L3 to L2. One explanation for the discrepancy between low L2S to L2S connectivity in (source-cell-specific) paired recordings and the high density of superficial inputs in our and another (source-cell-unspecific) mapping study would be that the superficial to superficial microcircuitry onto L2Ss is mainly established by L2Ps and L3Ps. Interestingly, the relative contribution of deep to superficial microcircuitry to a cell's functional input map is significantly larger for L2Ps than for L2Ss. Deep layer inputs integrate position, direction, and speed signals (Sargolini et al., 2006). We suggest that L2Ps receiving more ascending inputs might serve as integrative relays that convey spatial information to L2Ss.

The deep to superficial microcircuit is spatially organized in input clusters determined by the absolute position of the superficial target cell main axis. A detailed spatial analysis of these clusters with respect to the cell's main axis reveals patterns of microcircuit design that, to our knowledge, have not been described for other cortical areas. The size of these input clusters depends on the cell type of the target cell; the spatial spread of inputs from deep to superficial L2Ps and L3Ps is two times larger when compared to L2Ss. The deep input clusters projecting to L3Ps display a medial asymmetric offset to their main axis when compared to L2Ps and L2Ss.

A microcircuit has been defined as the "minimal number of interacting neurons that can collectively produce a functional output" (Grillner et al., 2005; Silberberg et al., 2005). Cells in the superficial layers of the MEC integrate position, direction, and speed signals to compute a grid-like matrix of external space, information that is then relayed to the hippocampus proper (Sargolini et al., 2006). The organization of superficial MEC microcircuitry described here is likely to be instrumental for this integrative computational task, which has already been speculated to be organized in spatially confined integrative units (Sargolini et al., 2006). The observed input clusters defined by the deep to superficial microcircuitry could constitute these integrative units at the microcircuit level. Future work will have to relate the specific patterns of microcircuit design to the systems and behavioral level function of integrative functional units in the MEC superficial layers.

EXPERIMENTAL PROCEDURES

Slice Preparation

Acute cortical slices were prepared from Wistar rats (age = postnatal day 15–25). Animals were anesthetized and decapitated. The brains were quickly removed and placed in ice-cold ACSF (pH 7.4) containing (in mM) 87 NaCl, 26 NaHCO3, 25 Glucose, 2.4 KCl, 7 MgCl2, 1.25 NaH2PO4, 0.5 CaCl2, and 75 Sucrose. Tissue blocks containing the brain region of interest were mounted on a vibratome (Leica VT 1200, Leica Microsystems, Wetzlar, Germany), cut at 300 μm thickness, and incubated at 35°C for 30 min. The slices were then transferred to ACSF containing (in mM): 119 NaCl, 26 NaHCO3, 10 Glucose, 2.5 KCl, 2.5 CaCl2, 1.3 MgSO4, and 1.25 NaH2PO4. The slices

were stored at room temperature in a submerged chamber for 1–5 hr before being transferred to the recording chamber.

Electrophysiology

Whole-cell voltage- and current-clamp recordings were performed with an Axopatch 700B Amplifier (Molecular Devices, Sunny Vale, CA, USA). Data were digitized (National Instruments BNC-2090, Austin, TX, USA) at 5 kHz, low-pass filtered at 2 kHz and recorded in a stimulation-point-specific manner with custom-made software.

For calibration experiments, patch electrodes (with electrode resistances ranging from 3–6 MΩ) were filled with (in mM): 135 K-gluconate, 20 KCl, 2 MgATP, 10 HEPES, 0.2 EGTA, and 5 phosphocreatine (final solution pH 7.3). For mapping experiments, the intracellular solution consisted of (in mM): 150 K-gluconate, 0.5 MgCl2, 1.1 EGTA, and 10 phosphocreatine (final solution pH 7.2). Initial access resistances were below 25MΩ after breakthrough and not allowed to vary more than 30% during the course of the experiment in the voltage-clamp mode. No access resistance compensation was used.

Glutamate Uncaging and Scanning of Glutamate-Evoked Activity

The setup and experimental procedures for photolysis of caged glutamate have been described previously (Bendels et al., 2008). For photostimulation and data acquisition, we used the Morgentau M1 microscope software (Morgentau Solutions, Munich, Germany). In brief, 20 ml of 200 μM 4-methoxy-7-nitroindolinyl-caged-l-glutamate (Tocris, Bristol, UK) were recirculated at 3–5 ml/min. The maximum time period of recirculation was 3 hr. The duration of the laser flash was 2 ms, the laser power under the objective, corresponding to the stimulus intensity levels used, was calibrated and constantly monitored with a photodiode array-based photodetector (PDA-K-60, Rapp Optoelectronics, Wedel, Germany). The optical system was adapted to achieve an effective light spot diameter of 15 μm in the focal plane. Generally, stimulation points were defined in a hexagonal grid with a raster size of 30 μm. For all experiments, the focal depth of the uncaging spot was set at 50 μm below the slice surface. To correct for differences in focal depth of the uncaging spot due to variability in slice surface height, we adjusted the focal depth for different subregions (Figure 2A). These subregions were scanned in a randomized order. All photostimulation experiments were done with inhibition intact as in our hands, blocking of inhibition with 2 μM of gabazine resulted in large depolarizing events (for details see Supplemental Experimental Procedures and Figure S2).

Histological Procedures

Slices with biocytin-filled cells were fixed in 0.1 mM phosphate buffer (pH 7.4) containing 4% paraformaldehyde for 24–48 hr. The filled neurons were visualized by incubating sections in avidin-biotin-conjugated horseradish peroxidase (ABC, Vector Laboratories, Ltd., UK) and reacting them with diaminobenzidine and hydrogen peroxide. Sections were then dehydrated and embedded on glass slides. Reconstruction and morphological analysis of the biocytin-labeled neurons were made with an Olympus BX61WI (Olympus, Hamburg, Germany) attached to a computer system (Neurolucida; Microbrightfield Europe, Magdeburg, Germany). Data were not corrected for tissue shrinkage. The reconstructed cells were superimposed onto the photomicrograph of the native slice with standard graphics software.

Analysis and Statistics

For detection of synaptic events, we used the automatic detection method described by Bendels et al. (2008). Parameters used for automatic detection were based on visual inspection of the raw data. The time window used for the detection of direct synaptic inputs was based on experiments blocking indirect synaptic inputs with TTX (Bendels et al., 2008). The postsynaptic current (PSC) rate of all experiments was plotted over time, and the duration of a photostimulation-induced significant increase in the PSC rate defined the time interval for the detection of indirect synaptic events. See Bendels et al. (2010) for a detailed description of the algorithm used for the separation of specific events constituting hotspots from background noise. In brief, specific photoactivation-induced inputs (synaptic points) were distinguished from randomly occurring background noise based on spatial correlations in spatially oversampled recordings. This procedure is validated by the observation that photostimulation results in the spatial clustering of hotspots in presynaptic cells (see Figures 1B–1E; Bendels et al., 2010). For quantifying the relative contribution of superficial and deep inputs, the percentage values representing the proportion of superficial and deep inputs were calculated for each individual cell. Subsequently, the overall percentage values were the averages of the percentage values for individual cells. For the spatial analysis of deep to superficial microcircuitry, only cells with more than five deep-layer synaptic points were included. The spatial distance was calculated in 30 μm bins. The main axis was set at 0. For calculation of the spatial spread, positive values were used for medial and lateral distances from the main axis. For calculation of the median distance of the input clusters from the main axis, medial distance was expressed in negative values and lateral distance was expressed in positive values. Statistical tests were performed with ANOVA, Mann-Whitney U Test, and Kruskal Wallis Test with Dunn's Multiple Comparison as a post-hoc test as appropriate. Numerical values are given as mean ± SEM.

SUPPLEMENTAL INFORMATION

Supplemental Information includes Supplemental Experimental Procedures and three figures and can be found with this article online at doi:10.1016/j.neuron.2010.12.009.

ACKNOWLEDGMENTS

This work was supported by the Deutsche Forschungsgemeinschaft/German National Research Council Grants Exc 257, SFB 618, SFB 665, BCCN Munich, and the Bernstein Focus, "Neuronal Basis of Learning." We thank Sarah Shoichet for critically reading an earlier version of the manuscript, Susanne Walden and Anke Schönherr for excellent technical assistance, and Isabelle Ommert for the Neurolucida reconstructions.

Accepted: November 29, 2010
Published: December 21, 2010

REFERENCES

Alonso, A., and Klink, R. (1993). Differential electroresponsiveness of stellate and pyramidal-like cells of medial entorhinal cortex layer II. J. Neurophysiol. *70*, 128–143.

Bendels, M.H., Beed, P., Leibold, C., Schmitz, D., and Johenning, F.W. (2008). A novel control software that improves the experimental workflow of scanning photostimulation experiments. J. Neurosci. Methods *175*, 44–57.

Bendels, M.H., Beed, P., Schmitz, D., Johenning, F.W., and Leibold, C. (2010). Detection of input sites in scanning photostimulation data based on spatial correlations. J. Neurosci. Methods *192*, 286–295.

Brivanlou, I.H., Dantzker, J.L., Stevens, C.F., and Callaway, E.M. (2004). Topographic specificity of functional connections from hippocampal CA3 to CA1. Proc. Natl. Acad. Sci. USA *101*, 2560–2565.

Callaway, E.M., and Katz, L.C. (1993). Photostimulation using caged glutamate reveals functional circuitry in living brain slices. Proc. Natl. Acad. Sci. USA *90*, 7661–7665.

Canto, C.B., Wouterlood, F.G., and Witter, M.P. (2008). What does the anatomical organization of the entorhinal cortex tell us? Neural Plast. *2008*, 381243.

Dalva, M.B., and Katz, L.C. (1994). Rearrangements of synaptic connections in visual cortex revealed by laser photostimulation. Science *265*, 255–258.

Dantzker, J.L., and Callaway, E.M. (2000). Laminar sources of synaptic input to cortical inhibitory interneurons and pyramidal neurons. Nat. Neurosci. *3*, 701–707.

Dhillon, A., and Jones, R.S. (2000). Laminar differences in recurrent excitatory transmission in the rat entorhinal cortex in vitro. Neuroscience *99*, 413–422.

Dickson, C.T., Mena, A.R., and Alonso, A. (1997). Electroresponsiveness of medial entorhinal cortex layer III neurons in vitro. Neuroscience *81*, 937–950.

Gloveli, T., Schmitz, D., Empson, R.M., Dugladze, T., and Heinemann, U. (1997). Morphological and electrophysiological characterization of layer III cells of the medial entorhinal cortex of the rat. Neuroscience *77*, 629–648.

Grillner, S., Markram, H., De Schutter, E., Silberberg, G., and LeBeau, F.E. (2005). Microcircuits in action—from CPGs to neocortex. Trends Neurosci. *28*, 525–533.

Iijima, T., Witter, M.P., Ichikawa, M., Tominaga, T., Kajiwara, R., and Matsumoto, G. (1996). Entorhinal-hippocampal interactions revealed by real-time imaging. Science *272*, 1176–1179.

Kloosterman, F., Van Haeften, T., Witter, M.P., and Lopes Da Silva, F.H. (2003). Electrophysiological characterization of interlaminar entorhinal connections: An essential link for re-entrance in the hippocampal-entorhinal system. Eur. J. Neurosci. *18*, 3037–3052.

Köhler, C. (1986). Intrinsic connections of the retrohippocampal region in the rat brain. II. The medial entorhinal area. J. Comp. Neurol. *246*, 149–169.

Kumar, S.S., Jin, X., Buckmaster, P.S., and Huguenard, J.R. (2007). Recurrent circuits in layer II of medial entorhinal cortex in a model of temporal lobe epilepsy. J. Neurosci. *27*, 1239–1246.

Lübke, J., and Feldmeyer, D. (2007). Excitatory signal flow and connectivity in a cortical column: Focus on barrel cortex. Brain Struct. Funct. *212*, 3–17.

Mountcastle, V.B. (1997). The columnar organization of the neocortex. Brain *120*, 701–722.

Sargolini, F., Fyhn, M., Hafting, T., McNaughton, B.L., Witter, M.P., Moser, M.B., and Moser, E.I. (2006). Conjunctive representation of position, direction, and velocity in entorhinal cortex. Science *312*, 758–762.

Schubert, D., Kötter, R., Zilles, K., Luhmann, H.J., and Staiger, J.F. (2003). Cell type-specific circuits of cortical layer IV spiny neurons. J. Neurosci. *23*, 2961–2970.

Schubert, D., Kötter, R., and Staiger, J.F. (2007). Mapping functional connectivity in barrel-related columns reveals layer- and cell type-specific microcircuits. Brain Struct. Funct. *212*, 107–119.

Shepherd, G.M., Pologruto, T.A., and Svoboda, K. (2003). Circuit analysis of experience-dependent plasticity in the developing rat barrel cortex. Neuron *38*, 277–289.

Silberberg, G., Grillner, S., LeBeau, F.E., Maex, R., and Markram, H. (2005). Synaptic pathways in neural microcircuits. Trends Neurosci. *28*, 541–551.

Witter, M.P., and Amaral, D.G. (2004). Hippocampal formation. In The rat nervous system, G. Paxinos, ed. (San Diego: Academic Press), pp. 637–703.